Research paper

Heat balance of senko-hanabi and iron sparks

Chihiro Inoue*†, Taiki Watanabe*, and Yuzo Inokuchi*

*Kyushu University, 744 Motooka, Nishi-ku, Fukuoka-shi, Fukuoka, 819-0395 JAPAN
Phone: +81-92-802-3018
†Corresponding author: inoue.chihiro@aero.kyushu-u.ac.jp

Received: March 15, 2019 Accepted: June 24, 2019

Abstract

Sparks emitted from the sparklers or the ground iron rods are luminous owing to the phenomenon of heat radiation. Hence, the colors of these sparks change depending on the temperature according to Planck's law. However, the mechanism of determining the temperature has not been clearly explained in a quantitative sense. Therefore, in the present study, we investigate two types of sparks, senko-hanabi, a traditionally popular Japanese sparkler, and ground iron spark, a well-known metal spark, using the two-color temperature radiometry technique and a theoretical analysis on heat balance. The temperature measurement clarifies that the temperature of sparks in a senko-hanabi is lower than that in the ground iron. The reason is revealed by the theoretical analysis that the heat production on a single spark of senko-hanabi is 40 mW, which is lower than that of iron spark as 50 mW, and the fusion of potassium sulfate consumes 40% of the heat produced on the sparks. We conclude that the fragile beauty of the senko-hanabi, attributed to the relatively low temperature, is realized by two factors, less heat production and the fusion of potassium sulfate.

Keywords: firework, spark, senko-hanabi, iron, temperature measurement, heat balance

1. Introduction

There are several types of sparklers enjoyed all over the world. Senko-hanabi (Figure 1) is one of the most popular sparklers in Japan since the Edo period (1603–1868). A senko-hanabi sparkler contains a "black powder", which is a mixture of charcoal, sulfur, and potassium nitrate in relative weight proportions of 15%, 25%, and 60%, respectively and does not comprise any metal powers[1]. This black powder is simply wrapped at one end of a twisted paper, being a 15 cm long thin paper string. One holds the top end of the paper string and ignites the lower end, upon which a red-hot globule appears, and sparks are emitted. The sparks travel downstream and eventually burst and ramify to show the pine needle-like shapes of fireworks.

In the past, Hoffmann[3] and Denisse[4] in Europe, and Terada[5] in Japan were intensely interested in the physical and chemical phenomena occurring in the senko-hanabi. Nakaya and Sekiguchi[6] initially identified that the sparkler retains the burning reaction using the ambient oxygen. Shimizu[1),7)] reported that potassium sulfide is an important reactive product in the sparks. Maeda and his high school students[8] conducted the chemical analyses and discovered several potassium compounds in the

Figure 1 Senko-hanabi[2]
The diameter of the twisted paper string is 2 mm. A globule forms at the bottom of the paper string. Sparks are emitted from this globule and reach up to several centimeters.

globule without potassium nitrate. This was because, potassium nitrate might quickly convert to other compounds soon after the ignition, which is consistent with Nakaya's findings[6]. Ito[9] estimated the crystal structure of the globule. Itoh et al.[10] conducted a spectroscopic study and confirmed the existence of

Figure 2 Ground iron sparks
The grinder on the left side rotates clockwise at a circumferential velocity of 30 m s^{-1}. By pressing the metal rod on the grinder, iron particles are ground, and sparks are emitted.

potassium ions inside the globule and the sparks. Recently, we have succeeded in capturing the resolved images, clearly identified that the sparkler undergoes a rate-controlled process owing to thermal diffusion, and eventually formulated the ramification cascade of the sparks[2),11),12)].

Several other sparklers usually contain metal powders, such as aluminum and magnesium. The senko-hanabi and the other sparklers, such as the ground iron sparks[13),14)], shown in Figure 2, are luminous owing to the heat radiated from the spreading tiny particles. However, we recognize that the sparks in the senko-hanabi exhibit a typical fragile beauty, which is not observed in the other types of sparklers. This fact indicates that the temperature and the heat balance characteristics might be different for various types of sparks. In this study, we demonstrate the findings with respect to the temperature measurements to reveal the coloration mechanism and discuss the heat balance characteristics of two different types of sparks in a quantitative sense.

2. Methods

We conduct the temperature measurements and theoretical analysis of two types of sparks, the senko-hanabi and ground iron-sparks. There is no oxidant contained inside the particles of the sparks. The senko-hanabi used in this study were produced by the Tsutsui-Tokimasa toy fireworks factory[15)] (Figure 3(a)). In addition, a pure iron rod and a carbon steel rod with the carbon concentration of 1 wt.% (Figure 3(b)) were ground to observe the iron sparks.

2.1 Temperature measurements

The color of the sparks emitted from both the senko-hanabi and the ground irons is the result of heat radiation according to Planck's law. The two-color temperature radiometry, an emissivity free measurement technique, was employed for measuring the temperatures. The instantaneous luminance ratio of red to green in every image pixel of the camera was converted to the respective

(a) Senko-hanabi
The black powder is wrapped at the right side of the paper string.

(b) Iron rods
Top: SUY is pure iron. Bottom: SK105 is carbon steel with 1 wt.% of carbon.

Figure 3 Materials used to produce sparks.

temperature values using a previously calibrated equation. As the lengths of the sparks in the senko-hanabi are in the range of $l \sim 10^{-2}$ m, a high-speed video camera, Photron SA-Z, was employed to perform the unsteady temperature measurements. However, the lengths of the iron sparks were much longer ($l \sim 10^{-1}$ m), we used SONY α 7sII, a high spatial resolution camera to measure the spark temperatures along the trajectory of the spark at every unit pixel.

2.2 Physical properties

It is important to consider some of the physical properties of the sparks while performing a quantitative calculation of their heat balance characteristics. A chemical reaction of the black powder produces a globule in the senko-hanabi[16)].

$$4KNO_3 + 7C + S \rightarrow 3CO_2 + 3CO + 2N_2 + K_2CO_3 + K_2S \quad (1)$$

The chemical reactions occurring inside the globule produce gas and other compounds[1),9)].

$$2K_2CO_3 + (2x+1)S \rightarrow 2K_2S_x + SO_2 + 2CO_2 \quad (2)$$
$$8K_2CO_3 + (3x+1)S_2 \rightarrow 6K_2S_x + 2K_2SO_4 + 8CO_2 \quad (3)$$
$$4K_2SO_4 + 7C \rightarrow 2K_2CO_3 + 2K_2S_2 + 5CO_2 \quad (4)$$

Initially contained 0.1 g (100 mg) of the black powder generates a lighter globule that weighs 30 mg by releasing the massive gases. The globule consists of K_2S_x, K_2CO_3, K_2SO_4, and C, as measured by Maeda[8)], in which the potassium compounds are in the states of molten salts or solid particles. Table 1 lists the main components of the globule. An exothermic reaction of the sparks on the surface of the globule continuously produces heat leading to a higher temperature of over 1000 K.

Table 1 Main components of the senko-hanabi globule[17]

Material		Melting point [K]	Density [kg m^{-3}]	Enthalpy of Fusion [kJ mol^{-1}]
potassium sulfide	K_2S	1113	1740	16.2
potassium carbonate	K_2CO_3	1164	2428	27.6
potassium sulfate	K_2SO_4	1342	2660	36.4
carbon	C	3915*	–	–

*decomposition (graphite as a reference)

$$C + O_2 = CO_2 \qquad \Delta H = -393\ [\mathrm{kJ\ mol^{-1}}] \qquad (5)$$

As the sparks observed in the senko-hanabi are ejected through a specific portion of the globule, we use the values listed in Table 1 to analyze the heat balance.

The iron particles are not covered with the oxide film immediately after they are ground. The oxidization reactions are exothermic and occur on the surface, given as follows:

$$Fe + 1/2\ O_2 = FeO \qquad \Delta H = -267\ [\mathrm{kJ\ mol^{-1}}] \qquad (6)$$
$$2Fe + 3/2\ O_2 = Fe_2O_3 \qquad \Delta H = -822\ [\mathrm{kJ\ mol^{-1}}] \qquad (7)$$

The heat production of $q \sim 500$ kJ O_2-mol^{-1} is rate-controlled by the molecular diffusion of oxygen in the boundary layer surrounding the particle. The melting point of pure iron is 1808 K, and that of carbon steel containing 1 wt.% of carbon is 1623 K[17].

3. Results and discussions

3.1 Spark temperature

Figure 4 shows the visualization results of the senko-hanabi and the corresponding instantaneous temperature distribution with a space resolution of 20 μm pixel^{-1} The temperature of the globule is determined according to the melting points of K_2S and K_2CO_3 by the heat source of carbon oxidization[2]. The results of the temperature measurements of the sparks observed as light streaks or light spots in Figure 4 are demonstrated.

Figure 5 presents the time-variant temperature values of the senko-hanabi sparks, in which each solid line indicates the result of one specific particle. The lifetime of the spark τ_{life} is defined as the time spent from its ejection out of the globule until the burst, determined by the thermal diffusion time scale[2] as follows:

$$\tau_{life} = \frac{(d/2)^2}{\alpha} \qquad (8)$$

where the particle diameter of the spark is $d \sim 10^{-4}$ m, and the thermal diffusivity is $\alpha \sim 10^{-6}$ m^2 s^{-1}. The time t is normalized by τ_{life} as follows:

$$t^* = \frac{t}{\tau_{life}} \qquad (9)$$

Therefore, $t^* = 0$ and $t^* = 1$ indicate the moments of the spark spreading from the globule and bursting, respectively. The temperature of the sparks increases continuously leading to a burst eventually at 1270 K–1330 K. The maximum temperature becomes close to the

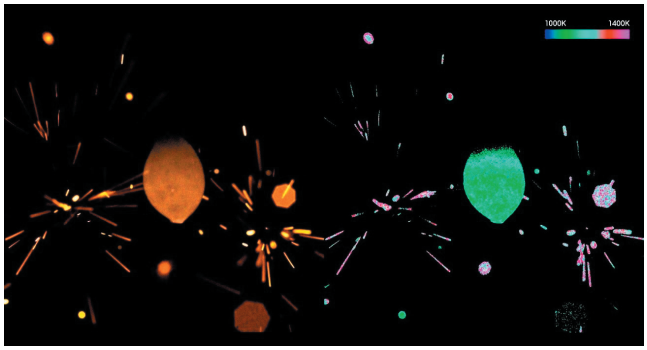

Figure 4 Visualized result (left) and temperature distribution (right).

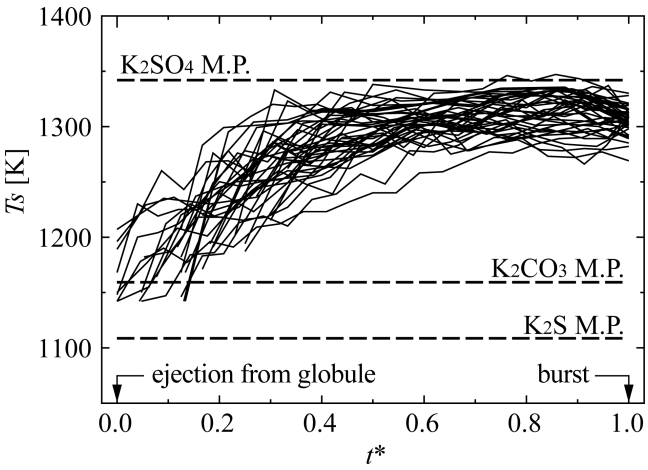

Figure 5 Temperature profile of senko-hanabi sparks from ejection to burst. (40 droplets were measured, reproduced from Ref. 2.)

melting point of K_2SO_4, indicating that the color of the sparks is strongly affected by the fusion of K_2SO_4. The flying velocity of the sparks is measured as $u \sim 10^0$ m s^{-1} [2]. Therefore, the distance from the globule to the bursting point is approximately $l \sim u \cdot \tau_{life} \sim 10^{-2}$ m.

The flying spark temperature of the ground carbon steel is shown in Figure 6. As the temperature close to the grinder was sufficiently low and the brightness was too weak to measure, the measurement position was approximately 100 mm downstream from the grinder. In the case of the pure iron spark, the temperature gradually increases passing the melting point of pure iron, as shown in Figure 6(a). This implies that the spark is in the solid phase initially and turns into a liquid later owing to the heat from the oxidization reaction represented by Equations (6) and (7). The temperature declines after reaching the maximum because of the heat dissipation

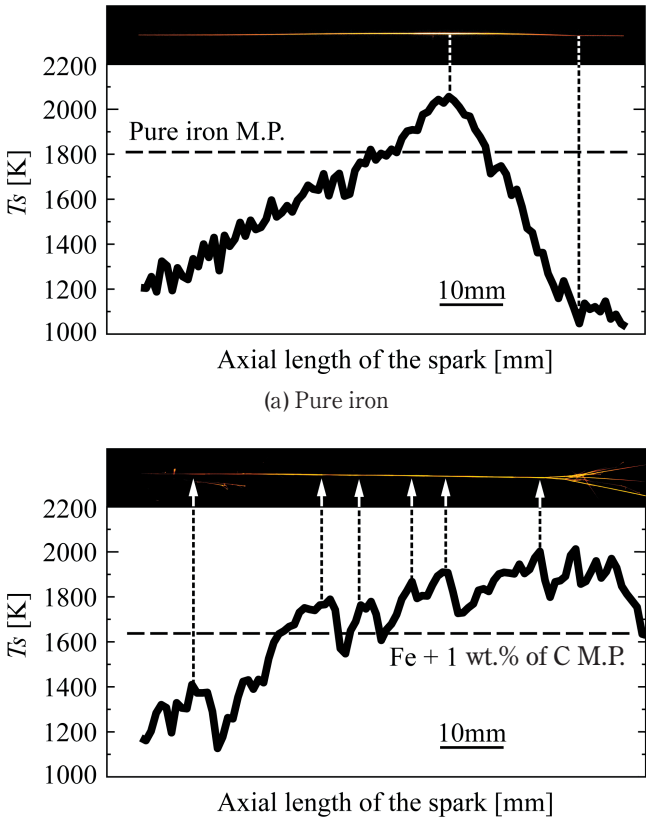

(a) Pure iron

(b) Carbon steel containing 1 wt.% of C

Figure 6 Temperature of the iron sparks. Top image shows a trajectory of the measured spark, spreading from left to right.

that occurred, as the oxidization heat is no longer produced after the particle surface is covered by iron oxide. In the case of carbon steel, the temperature gradually increases and the spark melts to a liquid, as shown in Figure 6(b). When the spark "puffs" observed as its expansion indicated by the arrows, the temperature synchronously increases. Since the puffing is caused by the existence of carbon[17], the temperature profile is different from that of the pure iron spark. However, the coincidence between the maximum temperatures of the pure iron and carbon steel sparks as T_s ~ 2000 K indicates that the oxidizations of iron are the most dominant heat source.

3.2 Heat balance

We calculate the heat balance of the sparks by considering the spark as a spherical particle with a typical diameter of $d = 10^{-1}$ mm. As the Nusselt number of the small particle is equal to 2, the boundary layer surrounding the particle is defined as $\delta \sim d/2$. For ambient air, the thermal conductivity is defined as $\lambda = 26$ mW m^{-1} K, molecular diffusion coefficient is $D = 1.8\times10^{-5}$ m^2 s^{-1}, oxygen concentration is $C = 8.9$ mol m^{-3}, and the temperature is $T_{air} = 288$ K. The enthalpy of fusion of K_2SO_4 is $L = 36.4$ kJ mol^{-1}. The overall heat balance under the steady state in unit time is formulated considering the term of heat production on the left-hand side and the respective terms of heat dissipation in the ambient air by heat transfer, radiation, and fusion on the right-hand side.

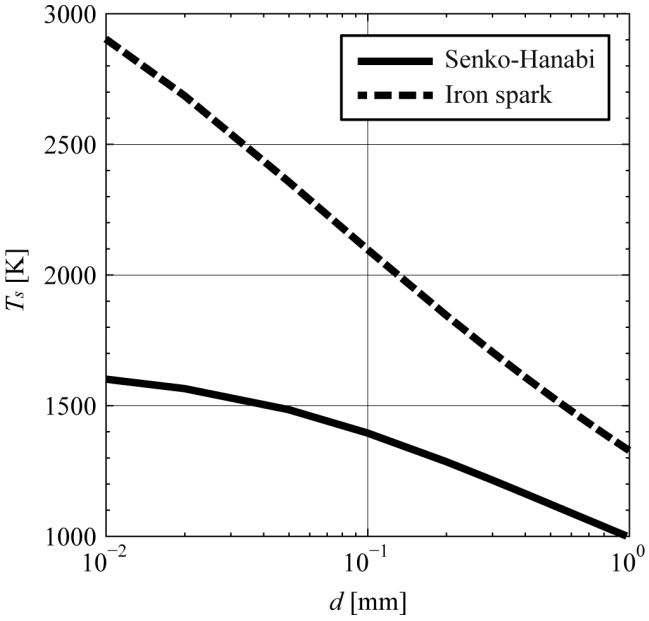

Figure 7 Calculated temperature of the sparks with variant d values.

$$D\frac{C}{\delta}q\cdot\pi d^2=\left(\lambda\frac{T_s-T_{air}}{\delta}+\sigma T_s^4\right)\cdot\pi d^2+\frac{m_{melt}}{M}\frac{L}{\tau_{life}} \quad (10)$$

where σ is the Stephan-Boltzmann constant, defined as $\sigma = 5.7\times10^{-8}$ W m^{-2} K^4, the emissivity is assumed to be unity, m_{melt} is the mass of the melting material, and M is the molar mass. For senko-hanabi sparks, approximately 20 wt.% of the particle (ρ ~ 2000 kg m^{-3}, refer to Table 1) comprises K_2SO_4[8], all of which are assumed to melt during τ_{life}. The heat balance of the senko-hanabi sparks is deduced as follows:

$$2\pi dDCq=2\pi d\lambda\,(T_s-T_{air})+\pi\sigma d^2T_s^4+\frac{2\pi}{15M}d\rho\alpha L \quad (11)$$

For ground iron sparks, the fusion term can be neglected at the steady state (around the maximum temperature), because the fusion is complete. The energy balance is then provided as follows:

$$2\pi dDCq=2\pi d\lambda\,(T_s-T_{air})+\pi\sigma d^2T_s^4 \quad (12)$$

We solve Equations (11) and (12) to obtain the temperature T_s at a specified d. The calculated results are shown in Figure 7. We find that the temperature of the iron spark is higher than that of the senko-hanabi spark, and the temperature of the smaller particles tends to be high. It is observed that at $d = 10^{-1}$ mm, $T_s = 2100$ K in the iron spark, and $T_s = 1390$ K in the senko-hanabi, which are consistent with the respective measurement values shown in Figure 5 and Figure 6. This confirms the validity of the heat balance analysis conducted. The agreement between the experimental and the analytical results also indicates that the frictional heat produced by the grinder demonstrates minimal effect on the iron spark temperature.

Figure 8 shows the absolute amount of heat at each term of Equation (10). As d increases, the sparks increase in size, resulting in larger surface area and volume, and

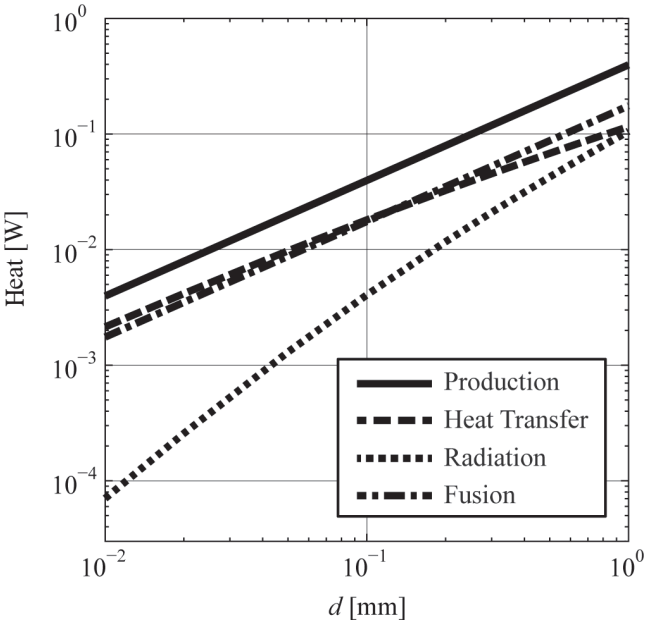

(a) Senko-hanabi

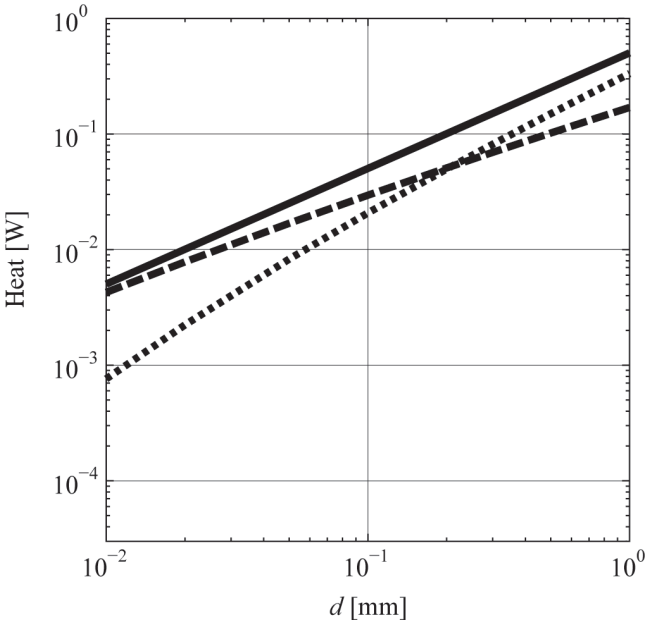

(b) Iron spark

Figure 8 Heat balance characteristics of the sparks.

therefore, the amount of heat tends to increase, as well. We observe the following difference between the two types of sparks: the fusion of K_2SO_4 is significant only in the senko-hanabi sparks, and the radiation is more dominant in the iron sparks. The amount of heat production is lower in the senko-hanabi sparks than in the iron sparks, because the heat production rate owing to the oxidization reactions defined in Equations (5) – (7) are lower in the senko-hanabi. The heat consumption ratio at $d = 10^{-1}$ mm is shown in Figure 9. The heat production of the senko-hanabi is 40 mW and that of the iron spark is 50 mW. The heat transfer to the ambient air and the fusion of K_2SO_4 are the most dominant factors, accounting for over 40% of the total heat consumption in the senko-hanabi, whereas the radiation only accounts for 10% of the heat consumption due to the relatively low temperature. With

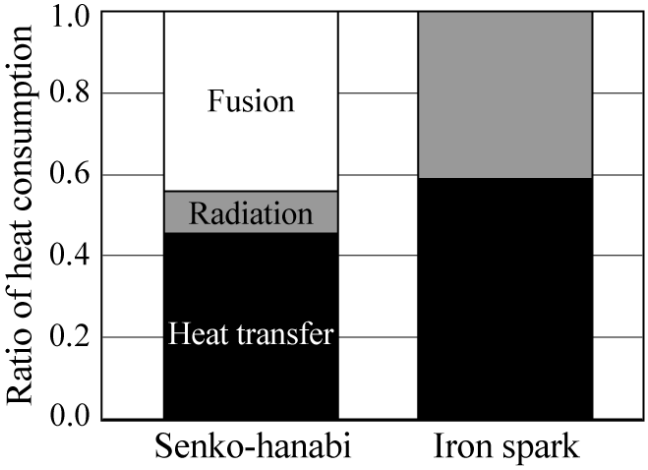

Figure 9 Ratio of heat consumption at $d = 10^{-1}$ mm. Total amount of heat consumption is equivalent to that of heat production, 40 mW in the senko-hanabi spark, and 50 mW in the iron spark, respectively.

respect to the iron sparks, the heat transfer attributes to 60% and the radiation consumes 40% of the total heat amount because of the higher temperatures (T_s = 2100 K). We conclude that the fragile beauty of the senko-hanabi, attributed to the relatively low temperature, is realized by two factors, less heat production and the fusion of K_2SO_4.

4. Conclusions

We measured the temperature of the sparks in the senko-hanabi and the ground iron using the two-color radiometry technique to reveal the heat balance in a quantitative sense. By comparing the experimental and theoretical results of these two types of sparks, we succeeded in identifying the differences in their temperature and the heat balance characteristics, which were the essence of the coloration mechanism. The temperature of the senko-hanabi sparks was observed to be lower than that of the iron sparks, because the heat production by carbon oxidization was lower than that due to the iron oxidization reactions, and the fusion of potassium sulfate in the senko-hanabi consumed 40% of the produced heat. These two factors contributed to the fragile beauty of the senko-hanabi sparklers observed since the Edo-period.

In this study, we investigated the well-known ground iron sparks to discuss the effect of the isolated metal powders. However, further analysis is necessary to clarify the coloration mechanism of the hand-holding type of sparklers that comprise a mixture of several metal powders and a strong oxidant.

Acknowledgement

This study was partially supported by KAKENHI (17H 00844 and 19K21934).

References

1) T. Shimizu, “Hanabi no Hanashi”, Kawade-Syobo (1976). (in Japanese).
2) C. Inoue, Y. Izato, A. Miyake, and E. Villermaux, Phys. Rev. Lett., 118, 074502 (2017).

3) A.W. Williamson, Chemical News, Dec. 24 (1864).
4) A. Denisse, Feux D'Artifice, Chap. 9 (1882).
5) T. Terada, "Terada Torahiko zuihitsu-syu", Iwanami-Bunko (1964). (in Japanese, originally written around 1927).
6) U. Nakaya and Y. Sekiguchi, Bulletin of the Institute of Physical and Chemical Research, 6, 1083−1103 (1927). (in Japanese).
7) T. Shimiz, J. Industrial Explosives Society (Sci. Tech. Energetic Materials), 18, 359−369 (1957). (in Japanese).
8) A. Maeda, et al., "Senko-Hanabi no kenkyu", Shinjuku High School (1962). (in Japanese).
9) H. Ito, Chemistry and Education, 39, 682−685 (1991). (in Japanese).
10) K. Itoh, D. Ding, and T. Yoshida, J. Pyrotechnics, 25, 14−27 (2007).
11) C. Inoue, M. Koshi, H. Terashima, T. Himeno, and T. Watanabe, Sci. Tech. Energetic Materials, 74, 106−111 (2013).
12) C. Inoue, M. Koshi, T. Himeno, and T. Watanabe, Sci. Tech. Energetic Materials, 77, 51−58 (2016).
13) J.C. Manson, Traité du fer et de l'acier (1804).
14) R.W. Buzzard, Bureau of Standards Research Paper, 11, 527−540 (1933).
15) Tsutsui Tokimasa Toy Fireworks, http://tsutsuitokimasa.jp/
16) M.S. Russell, "The Chemistry of Fireworks", Royal Society of Chemistry (2009).
17) D. L. Perry, "Handbook of Inorganic Compounds", CRC (2011).